BIOCHEMISTRY

The photoreactive free radical in eumelanin

Albertus B. Mostert,[1] Shermiyah B. Rienecker,[2,3] Christopher Noble,[2] Graeme R. Hanson,[2] Paul Meredith[4]*

Melanin is the primary photoprotecting pigment in humans as well as being implicated in the development of deadly melanoma. The material also conducts electricity and has thus become a bioelectronic model for proton-to-electron transduction. Central to these phenomena are its spin properties—notably two linked species derived from carbon-centered and semiquinone radicals. Using a novel in situ photoinduced electron paramagnetic resonance technique with simultaneous electrical measurements, we have elucidated for the first time the distinct photoreactivity of the two different radical species. We find that the production of the semiquinone is light- and water-driven, explaining the electrical properties and revealing biologically relevant photoreactivity.

INTRODUCTION

The melanins are a class of functional biomacromolecule found throughout nature in diverse roles including pigmentation, free radical scavenging, hard radiation protection, and even high-adhesive–strength structural components (*1*–*6*). The predominant and archetypal form of eumelanin (hereafter referred to as simply melanin) is the main photoprotectant in humans (*2*) but is also found in the substantia nigra of primates (as neuromelanin) (*7*), where it may serve as a chelator of potentially harmful transition metal ions (*8*, *9*). In what appears to be a direct contradiction of its photoprotective and free radical scavenger functions, melanin is also implicated in the development of deadly melanoma cancers of the eyes and skin (*4*, *10*). The photoreactivity of these pigments is thus a matter of considerable interest, and in this regard, natural and synthetic melanins have been shown to have almost unity nonradiative dissipation of absorbed ultraviolet and visible radiation (*11*). In addition, continuous wave (CW) electron paramagnetic resonance (EPR) has shed light on its spin properties, and a persistent, stable free radical appears to be a central feature of melanin physiochemistry (*2*). Finally, in what may be the most intriguing of its properties, melanin has been recently suggested to be a hybrid electrical conductor in the solid state (*12*). In these landmark experiments, it was demonstrated (*12*–*14*) that melanin is predominantly a proton conductor when suitably hydrated—an observation that broke several decades of misinterpretation of these materials as p-type amorphous "natural semiconductors" (*13*). This collection of optoelectronic properties has established melanins as model systems in the emerging field of bioelectronics (*15*) and, furthermore, stimulated renewed interest in finding biologically derived materials that can sustain macroscopic protonic and electronic conduction (*16*–*20*).

The underlying structure-property relationships that control many of these complex and diverse phenomena in melanins are not well understood (*2*). Structural disorder at the molecular and higher levels is, however, an accepted defining feature of melanin (*2*, *21*), as is its local reactivity with absorbed water (*12*, *22*). This latter feature is derived from the constituent molecular building blocks of melanin—indolequinones in various degrees of oxidation, cross-linked and organized into extended heteroaromatic sheets (*2*, *21*, *23*). The local reactions of water with hydroquinone and quinone moieties are thought to be governed by the equilibrium shown in Fig. 1: a relatively simple scheme termed the comproportionation equilibrium. It has been proposed that this reaction is the mechanistic origin of the macroscopic electrical conductivity. In this hypothesis, the production of hydronium equates to a population of labile protons able to diffuse through the hydrating water matrix via Grotthuss hopping (*12*, *14*, *22*). The addition of water shifts the equilibrium to the right by Le Chatelier's principle, effectively increasing free-carrier density. Furthermore, the comproportionation equilibrium may be the source of the transient and stable free radicals in melanin—the semiquinone (SQ) moiety is spin half, and its population should, in principle, also be hydration-modulated because the radical anion is protonated and deprotonated. Figure 1 also summarizes what may be termed the "light"-driven pathways. These pathways are somewhat speculative, particularly so the visible light–activated channel and its potential link to photoconductivity and biologically harmful photoreactivity. Figure 1 is further exemplified in the Supplementary Materials (see fig. S1 and Supplementary Text). Motivated by these basic questions regarding melanin structure-property relationships, we sought to link microscopic spin behavior (via EPR) with the macroscopic observable of electrical conductivity in a standard melanin synthetic model. We choose hydration and light irradiation as variable parameters to both validate the predictions of Fig. 1 and provide further insight with regard to photoreactivity.

RESULTS AND DISCUSSION

In the following discussion, it should be kept in mind that EPR spectra are conventionally presented as the first derivative of the absorption spectrum. Hence, analyses tend to focus on spectral features as proxies for radical behavior. Consequently, a distinction is made between the assigned *g* value (the value reflecting a radical's chemical nature) and *g* values of spectral features, which we will distinguish below.

The heterogeneity of melanin makes precise EPR signal assignment challenging (*12*, *14*, *24*, *25*). Several decades of EPR-melanin studies have delivered the following understanding regarding its EPR signal and relationship to radical species:

(i) In solution, the SQ radical (SQR) signal dominates the spectrum (assigned $g = 2.004$). This EPR signal is photoactive (*26*) and shows dependence on three factors—pH (*27*), metal ion chelation (*28*), and Arrhenius temperature dependence (*29*), all of which are reversible. Under high pH conditions in the solid state, the SQR is minimally observed as a distinct shoulder feature (*24*);

[1]Department of Chemistry, Swansea University, Singleton Park, Swansea, Wales SA2 8PP, UK. [2]Centre for Advanced Imaging, University of Queensland, St Lucia, Brisbane, Queensland 4072, Australia. [3]School of Chemistry and Molecular Biosciences, University of Queensland, St Lucia, Brisbane, Queensland 4072, Australia. [4]Department of Physics, Swansea University, Singleton Park, Swansea, Wales SA2 8PP, UK.
*Corresponding author. Email: paul.meredith@swansea.ac.uk

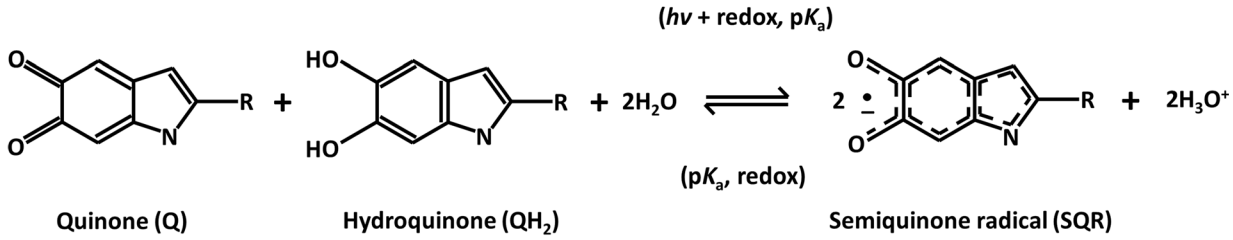

Fig. 1. Comproportionation equilibrium. Indolequinone moieties of different oxidative states react with water to form hydronium and an intermediate state, the SQR. The light-activated and dark mechanisms are summarized in the brackets. With light-activated reactions, light induces a redox reaction, followed by dissociation. For dark reactions, dissociation occurs first, followed by a redox reaction. For more details, see fig. S1 and Supplementary Text.

(ii) A carbon-centered radical (CCR) dominates the solid-state EPR signal (peak feature at g = 2.0049) (*14*, *24*) with no reported light dependence and an irreversible Curie-Weiss temperature dependence (*30*, *31*).

Hence, the challenge in using EPR as a probe for both radicals and particularly the SQR in the solid state is achieving spectral resolution of the SQR and CCR signals in the same sample while modulating their relative populations. To achieve sufficient spectral resolution of the EPR signal and overcome the CCR dominance in the solid state, we initially performed CW EPR experiments on melanin pressed powder pellets by varying the microwave power at X-band frequencies. This EPR technique is referred to as progressive power saturation and is often used to distinguish between two radical species with close g values. Distinct power saturation behaviors occur for the radicals because of their different responses to the microwave power, which are based on their characteristic spin-lattice relaxation times. This is exactly what we observe in the melanin power saturation experiment measured under neutral pH conditions, and the resultant spectra in Fig. 2 show that, at high microwave power (585 mW, orange spectrum), a second feature is observable at g = 2.0075. This additional feature is not present at low power (2 mW, black spectrum), which is characteristically the CCR (feature at g = 2.0049). We interpret the g = 2.0075 component as the SQR. We note that when measured with progressively higher microwave powers, it emerges, whereas the CCR saturates. The SQR signal can be further enhanced by exposing the sample to ammonia vapor (basic pH above the hydroquinone pK_a), which leads to the shoulder feature becoming the dominant peak because more SQR moieties are formed according to Fig. 1. Similar power saturation effects have been observed in polydopamine systems at moderate microwave powers (approximately 160 mW) (*32*). This power saturation/pH result establishes a basis by which we can observe the relative concentrations of the two melanin free radicals.

Turning now to controlled hydration and irradiation, it is well established that both the dark and photoconductivity of melanin and the shape of the EPR spectrum are heavily influenced by the degree of hydration particularly above ~10% by weight (*12*–*14*, *24*). We have previously reported a custom-built vapor delivery system, which allows in situ EPR measurements to be performed (*14*, *24*). We coupled this system to an adapted EPR resonance cavity by mounting a white light-emitting diode (LED) source to allow coupling of visible radiation, yielding a system that can simultaneously control light, microwave power, and hydration. This cavity yielded optimal microwave powers of 199.2 and 0.063 mW to probe the SQR and CCR species, respectively. More information on these optimizations is provided in the Supplementary Materials. The dark spectra of neutral pH samples (fig. S2) show the same qualitative behavior as Fig. 2—the emergence of the

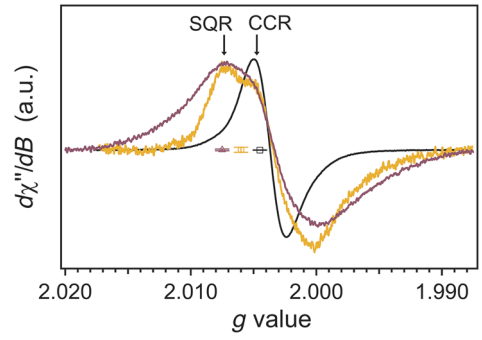

Fig. 2. Melanin X-band EPR spectrum obtained under vacuum (that is, dry). The black and orange curves are at microwave powers of 2 and 585 mW, respectively. The purple curve (585 mW) was obtained after exposure to ammonia vapor and dried under vacuum. It can be seen that the peak at g = 2.0049 is reduced with increasing microwave power, whereas a peak at g = 2.0075 emerges. The addition of base increases the relative strength of the g = 2.0075 peak, thus showing that the strength of the SQ free radical signal (g = 2.0075) can be enhanced vis-à-vis the carbon-centered free radical signal (g = 2.0049). Uncertainties shown indicate the noise in the baseline. a.u., arbitrary units.

SQR at higher microwave powers and the dominant CCR at low power. In addition, we observe that the CCR signal intensity shows a relatively uniform decrease from dry (0% weight gain) to hydrated (17.2% weight gain). In contrast, and consistent with previous observations (*24*), the SQR signal intensity is relatively unaffected—a consequence of the compensatory combination of the CCR decreasing and SQR increasing (*12*). By focusing on the spectral features of the CCR and SQR (g values assigned from fig. S2), we obtained time traces at different hydrations with the light source (LED spectrum; fig. S3) switched on at defined times.

Photo-EPR time traces optimized for the CCR are shown in Fig. 3A, and we note an intriguing negative photosignal for the dry case (black curve)—this is associated with the creation of SQR induced by the illumination and hence a reduction in the CCR intensity. This occurs even "dry," although we note that solid-state melanin always contains a fraction of strongly bound water even when pumped to vacuum (*33*). The light-on and light-off points are marked on the traces. Because the melanin sample was exposed to water, the CCR photosignal flattened (blue) and then changed to a positive at high water contents (red). In contrast, the SQR time traces (Fig. 3B) were qualitatively different. At all hydrations, a positive photo-EPR signal was observed, consistent with an overall increase in the SQR concentration. Thus, Fig. 3 constitutes additional and explicit proof of two different free radical populations in melanin—we believe the first such observation seen in the same sample and experiment.

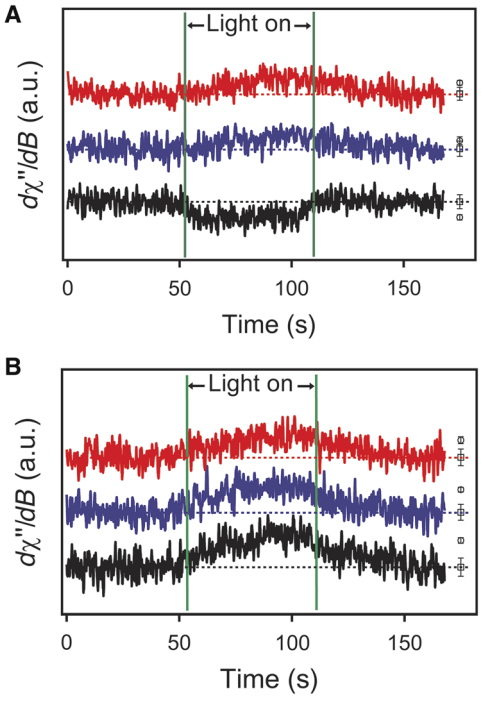

Fig. 3. Photo-EPR time traces for neutral melanin. (**A**) Photo-EPR time traces at 0.063-mW microwave power and monitored at g = 2.0049, the CCR feature. The colors indicate hydration state, which was obtained by normalizing the vapor pressure to a previously published adsorption isotherm (*33*): 0% (black), 11.6% (blue), and 17.2% (red) weight gain in water relative to melanin dry mass. Traces have been offset from one another for clarity. Dashed lines indicate baseline before the light is switched on. (**B**) Photo-EPR time trace at 199.2 mW and positioned at g = 2.0075, the SQR feature. Data point markers indicate the mean and uncertainties in the baseline (squares) and the signal (circles).

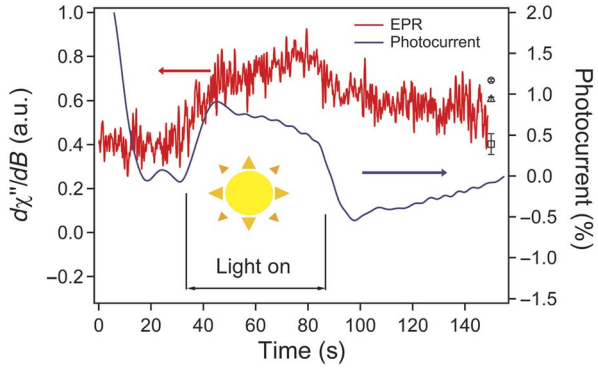

Fig. 4. Representative photo-EPR time trace (optimized for the SQR, 11.6% weight gain in water content) overlaid on a photocurrent time trace obtained for a contacted melanin sample and obtained simultaneously in situ. The data confirm that the SQ free radical is explicitly linked to the conductivity and hence the protonic conducting behavior of solid-state melanin. Data point markers indicate the mean and uncertainties in the initial baseline (square), the signal (circle), and the final baseline (triangle).

The similar photo-EPR signals of the SQR at different hydrations (Fig. 3B) are likely due to a saturation effect where the maximum amount of photoinduced SQRs was already generated at the lowest hydration level. As for the data obtained under optimal EPR measurement parameters for the CCR (Fig. 3A), the increasingly positive photo-EPR signals at the CCR peak appear to be from the influence of the superimposed SQR signal that becomes more prominent at higher hydration levels (according to Fig. 1).

Finally, we performed a simultaneous hydration-dependent photo-EPR/photoconductivity measurement. This requires electrical contacting in a geometry that does not alter the quality factor of the EPR cavity and allows for hydration of the melanin sample and sufficient signal to noise. Details of this procedure are provided in Materials and Methods. We also replicated the CW EPR measurements above for the contacted samples (see the Supplementary Materials and fig. S4) to check the possible impact of the contacts on the cavity and the consistency between the two data sets.

Thus, we show in Fig. 4 a representative photoconductivity and photo-EPR data set optimized for the SQR signal and obtained in situ simultaneously. Critically, the SQR photo-EPR time trace coincides with the photocurrent time trace. Other examples (at different hydrations) are provided in the Supplementary Materials for completeness (figs. S5 to S8). Recalling that the current in melanin is predominantly protonic, Figs. 3 and 4 thus constitute explicit proof of the link between proton transport and the SQ free radical produced via hydration and visible light irradiation. The CCR does not appear to contribute in any way to the photocurrent due to its anticorrelative behavior, seen for example in fig. S8. The data presented here do not rule out the existence of additional free radical species in melanin, but it does, for the first time, demonstrate explicitly the presence of at least two different radical species.

One variable that can influence the light-induced free radical properties is the aggregation properties of the melanin polymer. It is currently an open question as to how aggregation proceeds during synthesis (*34*) and how exactly aggregation is involved in photoprotection (*35*), although there is no doubt that it could play a role. It is also known that the state of aggregation and the structures formed during synthesis are dependent on the ratio of monomer units (dihydroxyindole and dihydroxyindole carboxylic acid) in the reactant mix, which, in turn, also affects the EPR spectra (*36*). Our clear intent in using a standard synthetic model, which broadly represents the family that is melanin, is to establish a baseline radical population analysis from which many more variables can be probed—aggregation being one.

Finally, we note that the behavior of the baseline current and EPR signals before, during, and after light irradiation are different. These effects and their differences are subtly related to phenomena, such as the contact nature of the macroscopic conductivity measurements (and the noncontact nature of EPR), plus the relative sensitivities to hydration and sample temperature, which deliver baseline drift and differences in response times. We expand upon these subtleties in the Supplementary Materials for completeness and as guidelines for how to interpret baseline versus significant induced effects in melanin solid-state electrical spectroscopy.

CONCLUSION

In conclusion, using novel in situ hydration and photo-EPR in X-band power saturation mode, we have provided compelling evidence for the existence of two free radical populations in a standard synthetic model of the important functional biomacromolecule melanin. The transient SQR species produced by the coupled reactions of the comproportionation equilibrium is directly involved in protonic electrical conductivity. It is interesting to speculate as to whether this mechanism is generic in the solid state for all suitably "proton-active" conducting biomaterials

containing groups such as hydroquinones with pK_as around neutral. Furthermore, our photo-EPR data reveal pronounced photoreactivity under visible light irradiation of moderate intensities. Given melanin's role in photo-driven processes in nature, this is both potentially concerning and also offers a new perspective on its various functions in, for example, vision as a photoreceptor, and other neural signaling pathways. More generically, protonated SQs are also known to be involved in photosynthetic reaction centers, such as bacterial reaction centers, which involves protonating/deprotonating the SQR. The methodologies we describe here have wide application to biological photoactivity studies.

MATERIALS AND METHODS

Synthesis of melanin

Melanin synthesis was performed according to the standard procedures (*28*, *33*). Five grams of DL-dopa purchased from Sigma-Aldrich was dissolved in 2 liters of Millipore water. Ammonia solution (28%) was added to adjust the solution to pH 8. The solution was then bubbled with compressed air for 3 days, after which the color changed from clear to brown-black. The melanin was precipitated out of solution by adjusting to pH 2 with the addition of hydrochloric acid (32%). The precipitate was filtered and washed three times with Millipore water before drying in an oven at 80°C overnight.

Sample preparation

The samples were prepared using a method previously published (*33*). In summary, 200 mg of dry melanin was crushed to a fine powder and pressed into a pellet using a manual hydraulic press under 80 tons of pressure for 5 min. The resulting pellet had a diameter of 13 mm and a thickness of approximately 1 mm. It was then cut into pieces suitable for fitting standard X-band CW EPR quartz tubes. For the simultaneous conductivity and EPR measurements, the two largest faces of the pellet were first evaporated with gold (100 nm) and then connected to copper wires using silver epoxy.

High-power EPR

The initial high-power controlled experiment (Fig. 2) was performed using a vacuum line setup previously reported (*12*, *24*). X-band EPR measurements were performed on a Bruker ELEXSYS E500 CW EPR spectrometer using a Bruker ER4122 super-high-Q cavity with a liquid nitrogen flow insert (controlled by a Eurotherm 4131VT variable temperature controller, which maintained the sample at 296 K). A Bruker Teslameter (ER036M) and an EIP 548B frequency counter were used to provide calibration of the magnetic field and microwave frequencies, respectively. A spectrum was then taken at 2 mW (the optimal signal to noise for the CCR component) and 585 mW (the highest power output achievable with the power leveler off to saturate the CCR as much as possible). To obtain the high-pH spectrum, we initially exposed the sample under vacuum to an ammonia atmosphere via an attached vial of ammonia (28% concentration), leaving the system to come to equilibrium overnight. Afterward, the sample was evacuated for about 10 min to recreate a vacuum, and the spectrum was taken again at 585 mW.

Hydration-dependent CW and photo-EPR

We used a Bruker 4119HS-W1 optical resonator with an optical window to expose the sample in the cavity to a white LED light source. The white LED source was mounted on a passive cooling radiator to ensure consistency of performance over time and was run at approximately 3.5 W of input power using a Keithley 2400 source meter unit (sourcing 1 A). The LED emission spectrum is shown in fig. S3. X-band CW EPR spectra (dark signals) were obtained at 0.063 mW of microwave power (to achieve optimal signal to noise for the CCR without saturating the signal). The highest microwave power achievable (199.2 mW) was used to measure the SQR while suppressing the CCR signal as much as possible (figs. S2 and S4). Hydration control was achieved by attaching a water vial (Millipore; freeze-thaw–pumped three times) to the vacuum line with a suitable valve to achieve the desired water vapor pressure as measured by a BOC-Edwards GK series (0-50 mbar gauge). Using a previously published adsorption isotherm (*33*), the pressures measured were converted to weight percent gained of water in terms of melanin mass. For the photo-EPR experiments, the CW EPR spectrum signal intensity was initially optimized for the CCR or SQR component (at a given hydration and selecting either 0.063- or 199.2-mW microwave power) and measured with 0.25-G modulation amplitude. Once obtained, the g value was set to the peak position of either the CCR (g = 2.0049) or the SQR (g = 2.0075). A time-based signal was then acquired for approximately 165 s. To compensate for any EPR signal intensity drift as a function of time, we used a field-frequency lock method in conjunction with the Teslameter to ensure that the same field position was maintained over the course of the experiment. During the time scan, the first 50 s was obtained under dark conditions with the following 50 s of the sample being exposed to the white LED. The rest of the scan was then acquired in the dark.

Hydration-dependent photo-EPR/photoconductivity

Melanin samples were prepared by contacting two opposing sides with thermally evaporated gold (100 nm) and copper wiring attached with silver epoxy. The wiring was connected to a custom-made vacuum electrical plug (*12*) to enable outside connection. Otherwise, the vacuum system used was the same as for all other experiments. The basic procedures for obtaining the photo-EPR measurements were also the same as stated above. However, because of the electrical contacts reducing the available photoactive surface area of the sample, the signal-to-noise ratio (SNR) was significantly lower. Thus, we improved the SNR by increasing the modulation amplitude to 9.8 G, which produced the same qualitative behavior observed (compare Fig. 3 and fig. S5) with an acceptable level of line broadening. Note that the CW EPR data shown in fig. S4 are dark spectra of the electrically contacted samples measured using the above 0.25-G modulation amplitude for comparison to the uncontacted samples (fig. S2). In short, the electrical contacted samples showed the same qualitative features as presented here and are in accordance with previously published results.

Photoconductivity data were obtained simultaneously with the photo-EPR signal by observing the current as measured by a Keithley 2450 source meter unit applying 15 V. We note that, at low microwave power (0.063 mW), obtaining a photoconductivity signal was not an issue and with no observable signal at vacuum (due to lack of charge carriers) and clear signals observed at wetter atmospheres. Behaviors were in line with previously reported studies (*13*), including observed negative conductivities due to dehydration effects. However, we discovered that, at high microwave power (199.2 mW) and high hydration, the electrical noise made the photoconductivity signal unobservable. Only at the medium hydration level (11.6% weight gain) was a signal observed, but with ringing behavior. Consequently, the data were filtered using a low-pass third-order Butterworth filter using MATLAB.

Uncertainty/noise analysis of EPR time traces and CW EPR spectra

The uncertainties in the initial baselines were determined by calculating the root mean square/uncertainty value of the traces/baseline by

$$\sigma = \sqrt{P_{\text{noise}}}$$

where P_{noise} is the power of the noise of the baseline and is determined by the basic power equation

$$P = \frac{1}{T}\int_0^T s(t)^2 dt$$

where $s(t)$ is the signal and T is the time period of observation. In determining the uncertainty in the EPR time-trace signal, the definition of the SNR was used

$$\text{SNR} = \frac{P_{\text{signal}}}{P_{\text{noise}}}$$

Once determined, the uncertainty was given by the mean of the signal multiplied by 1/SNR.

SUPPLEMENTARY MATERIALS

Supplementary material for this article is available at http://advances.sciencemag.org/cgi/content/full/4/3/eaaq1293/DC1

Supplementary Text

fig. S1. Proposed comproportionation reaction pathways.

fig. S2. CW EPR spectra for neutral melanin.

fig. S3. Emission spectrum of the white LED light source.

fig. S4. CW EPR spectra for electrically contacted melanin samples.

fig. S5. Photo-EPR time traces of electrically contacted melanin samples.

fig. S6. Photoconductivity measurements taken at the same time as the EPR time traces in fig. S5A.

fig. S7. In situ simultaneous photo-EPR/photoconductivity data observed on neutral samples, but under ambient conditions.

fig. S8. In situ simultaneous photo-EPR/photoconductivity data observed on neutral samples, as a function of hydration.

References (*37*–*54*)

REFERENCES AND NOTES

1. G. Prota, *Melanins and Melanogenesis* (Academic Press, 1992).
2. P. Meredith, T. Sarna, The physical and chemical properties of eumelanin. *Pigment Cell Res.* **19**, 572–594 (2006).
3. T. Sarna, B. Pilas, E. J. Land, T. G. Truscott, Interaction of radicals from water radiolysis with melanin. *Biochim. Biophys. Acta* **883**, 162–167 (1986).
4. J. Y. Lin, D. E. Fisher, Melanocyte biology and skin pigmentation. *Nature* **445**, 843–850 (2007).
5. E. Dadachova, R. A. Bryan, X. Huang, T. Moadel, A. D. Schweitzer, P. Aisen, J. D. Nosanchuk, A. Casadevall, Ionizing radiation changes the electronic properties of melanin and enhances the growth of melanized fungi. *PLOS ONE* **2**, e457 (2007).
6. H. Lee, S. M. Dellatore, W. M. Miller, P. B. Messersmith, Mussel-inspired surface chemistry for multifunctional coatings. *Science* **318**, 426–430 (2007).
7. W. D. Bush, J. Garguilo, F. A. Zucca, A. Albertini, L. Zecca, G. S. Edwards, R. J. Nemanich, J. D. Simon, The surface oxidation potential of human neuromelanin reveals a spherical architecture with a pheomelanin core and a eumelanin surface. *Proc. Natl. Acad. Sci. U.S.A.* **103**, 14785–14789 (2006).
8. F. A. Zucca, G. Giaveri, M. Gallorini, A. Albertini, M. Toscani, G. Pezzoli, R. Lucius, H. Wilms, D. Sulzer, S. Ito, K. Wakamatsu, L. Zecca, The neuromelanin of human substantia nigra: Physiological and pathogenic aspects. *Pigment Cell Res.* **17**, 610–617 (2004).
9. L. Hong, J. D. Simon, Current understanding of the binding sites, capacity, affnity, and biological significance of metals in melanin. *J. Phys. Chem. B* **111**, 7938–7947 (2007).
10. V. Gray-Schopfer, C. Wellbrock, R. Marais, Melanoma biology and new targeted therapy. *Nature* **445**, 851–857 (2007).
11. P. Meredith, J. Riesz, Radiative relaxation quantum yields for synthetic eumelanin. *Photochem. Photobiol.* **79**, 211–216 (2004).
12. A. B. Mostert, B. J. Powell, F. L. Pratt, G. R. Hanson, T. Sarna, I. R. Gentle, P. Meredith, Role of semiconductivity and ion transport in the electrical conduction of melanin. *Proc. Natl. Acad. Sci. U.S.A.* **109**, 8943–8947 (2012).
13. A. B. Mostert, B. J. Powell, I. R. Gentle, P. Meredith, On the origin of electrical conductivity in the bio-electronic material melanin. *Appl. Phys. Lett.* **100**, 093701 (2012).
14. S. B. Rienecker, A. B. Mostert, G. Schenk, G. R. Hanson, P. Meredith, Heavy water as a probe of the free radical nature and electrical conductivity of melanin. *J. Phys. Chem. B* **119**, 14994–15000 (2015).
15. M. Muskovich, C. J. Bettinger, Biomaterials-based electronics: Polymers and interfaces for biology and medicine. *Adv. Healthc. Mater.* **1**, 248–266 (2012).
16. D. D. Ordinario, L. Phan, W. G. Walkup IV, J.-M. Jocson, E. Karshalev, N. Hüsken, A. A. Gorodetsky, Bulk protonic conductivity in a cephalopod structural protein. *Nat. Chem.* **6**, 596–602 (2014).
17. C. Zhong, Y. Deng, A. F. Roudsari, A. Kapetanovic, M. P. Anantram, M. Rolandi, A polysaccharide bioprotonic field-effect transistor. *Nat. Commun.* **2**, 476 (2011).
18. Y. Deng, E. Josberger, J. Jin, A. F. Roudsari, B. A. Helms, C. Zhong, M. P. Anantram, M. Rolandi, H^+-type and OH^--type biological protonic semiconductors and complementary devices. *Sci. Rep.* **3**, 2481 (2013).
19. N. Amdursky, X. Wang, P. Meredith, D. D. C. Bradley, M. M. Stevens, Long-range proton conduction across free-standing serum albumin mats. *Adv. Mater.* **28**, 2692–2698 (2016).
20. P. Meredith, C. J. Bettinger, M. Irimia-Vladu, A. B. Mostert, P. E. Schwenn, Electronic and optoelectronic materials and devices inspired by nature. *Rep. Prog. Phys.* **76**, 034501 (2013).
21. M. d'Ischia, A. Napolitano, V. Ball, C.-T. Chen, M. J. Buehler, Polydopamine and eumelanin: From structure–property relationships to a unified tailoring strategy. *Acc. Chem. Res.* **47**, 3541–3550 (2014).
22. J. Wünsche, Y. Deng, P. Kumar, E. Di Mauro, E. Josberger, J. Sayago, A. Pezzella, F. Soavi, F. Cicoira, M. Rolandi, C. Santanto, Protonic and electronic transport in hydrated thin films of the pigment eumelanin. *Chem. Mater.* **27**, 436–442 (2015).
23. A. A. R. Watt, J. P. Bothma, P. Meredith, The supramolecular structure of melanin. *Soft Matter* **5**, 3754–3760 (2009).
24. A. B. Mostert, G. R. Hanson, T. Sarna, I. R. Gentle, B. J. Powell, P. Meredith, Hydration-controlled X-band EPR spectroscopy: A tool for unravelling the complexities of the solid-state free radical in eumelanin. *J. Phys. Chem. B* **117**, 4965–4972 (2013).
25. A. Batagin-Neto, E. S. Bronze-Uhle, C. F. d. O. Graeff, Electronic structure calculations of ESR parameters of melanin units. *Phys. Chem. Chem. Phys.* **17**, 7264–7274 (2015).
26. R. J. Sever, F. W. Cope, B. D. Polis, Generation by visible light of labile free radicals in the melanin granules of the eye. *Science* **137**, 128–129 (1962).
27. S.-S. Chio, J. S. Hyde, R. C. Sealy, Paramagnetism in melanins: pH dependence. *Arch. Biochem. Biophys.* **215**, 100–106 (1982).
28. C. C. Felix, J. S. Hyde, T. Sarna, R. C. Sealy, Interactions of melanin with metal ions. Electron spin resonance evidence for chelate complexes of metal ions with free radicals. *J. Am. Chem. Soc.* **100**, 3922–3926 (1978).
29. S.-S. Chio, J. S. Hyde, R. C. Sealy, Temperature-dependent paramagnetism in melanin polymers. *Arch. Biochem. Biophys.* **199**, 133–139 (1980).
30. M. S. Blois, A. B. Zahlan, J. E. Maling, Electron spin resonance studies on melanin. *Biophys. J.* **4**, 471–490 (1964).
31. P. J. Gonçalves, O. B. Filho, C. F. O. Graeff, Effects of hydrogen on the electronic properties of synthetic melanin. *J. Appl. Phys.* **99**, 104701 (2006).
32. N. F. D. Vecchia, A. Luchini, A. Napolitano, G. D'Errico, G. Vitiello, N. Szekely, M. d'Ischia, L. Paduano, Tris buffer modulates polydopamine growth, aggregation, and paramagnetic properties. *Langmuir* **30**, 9811–9818 (2014).
33. A. B. Mostert, K. J. P. Davy, J. L. Ruggles, B. J. Powell, I. R. Gentle, P. Meredith, Gaseous adsorption in melanins: Hydrophilic biomacromolecules with high electrical conductivities. *Langmuir* **26**, 412–416 (2010).
34. M. Arzillo, G. Mangiapia, A. Pezzella, R. K. Heenan, A. Radulescu, L. Paduano, M. d'Ischia, Eumelanin buildup on the nanoscale: Aggregate growth/assembly and visible absorption development in biomimetic 5,6-dihydroxyindole polymerization. *Biomacromolecules* **13**, 2379–2390 (2012).
35. A. Corani, A. Huijser, A. Iadonisi, A. Pezzella, V. Sundström, M. d'Ischia, Bottom-up approach to eumelanin photoprotection: Emission dynamics in parallel sets of water-soluble 5,6-dihydroxyindole-based model systems. *J. Phys. Chem. B* **116**, 13151–13158 (2012).
36. L. Panzella, G. Gentile, G. D'Errico, N. F. D. Vecchia, M. E. Errico, A. Napolitano, C. Carfagna, M. d'Ischia, Atypical structural and π-electron features of a melanin polymer that lead to

superior free-radical-scavenging properties. *Angew. Chem. Int. Ed.* **52**, 12684–12687 (2013).
37. J. Sunkel, H. Staude, Der Einfluß von Dissoziation und Substitution auf die physikalischen Eigenschaften von Dioxybenzolen 1. Mitteilung: Dissoziationskonstanten, Dissoziationsstufen, Redoxpotentiale und Dipolmomente. *Berichte* **72**, 567–573 (1968).
38. B. L. Trumpower, *Function of Quinones in Energy Conserving Systems* (Academic Press, 1982).
39. J. A. Pederson, *Handbook of EPR Spectra from Natural and Synthetic Quinones and Quinols* (CRC Press, 1985).
40. J. A. Pederson, On the application of electron paramagnetic resonance in the study of naturally occuring quinones and quinols. *Spectrochim. Acta A* **58**, 1257–1270 (2002).
41. V. A. Roginsky, L. M. Pisarenko, W. Bors, C. Michel, The kinetics and thermodynamics of quinone-semiquinone-hydroquinone systems under physiological conditions. *J. Chem. Soc.* **2**, 871–876 (1999).
42. M. Flores, M. Y. Okamura, J. Niklas, M.-E. Pandelia, W. Lubitz, Pulse Q-band EPR and ENDOR spectroscopies of the photochemically generated monoprotonated benzosemiquinone radical in frozen alcoholic solution. *J. Phys. Chem. B* **116**, 8890–8900 (2012).
43. N. K. Bridge, G. Porter, Primary photoprocesses in quinones and dyes. I. Spectroscopic detection of intermediates. *Proc. R. Soc. Lond. Ser. A* **244**, 259–275 (1958).
44. T. E. Gough, Solvation spectra. Part 15.—Dependence of e.s.r. spectra of monoprotonated semiquinones upon solvent. *Trans. Faraday Soc.* **62**, 2321–2326 (1966).
45. R. Das, B. Venkataraman, Hydrogen abstraction from solvents by the triplet state of p-benzoquinone: A time-resolved electron paramagnetic resonance and laser flash photolysis study. *Res. Chem. Intermed.* **31**, 167–192 (2005).
46. R. Arnaud, G. Perbet, A. Deflandre, G. Lang, Electron spin resonance of melanin from hair. Effects of temperature, pH, and light irradiation. *Photochem. Photobiol.* **38**, 161–168 (1983).
47. T. Sarna, R. C. Sealy, Free radicals from eumelanins: Quantum yields and wavelength dependence. *Arch. Biochem. Biophys.* **232**, 574–578 (1984).
48. M. Zdybel, B. Pilawa, Effect of UV irradiation on free radicals in synthetic melanin and melanin biopolymer from *Sepia officinalis*—EPR examination. *Nukleonika* **60**, 483–488 (2015).
49. F. W. Cope, R. J. Sever, B. D. Polis, Reversible free radical generation in the melanin granules of the eye by visible light. *Arch. Biochem. Biophys.* **100**, 171–177 (1963).
50. K. Loth, M. Andrist, F. Graf, H. H. Günthard, Modulated excitation ESR spectra of hydroxy-phenoxy radicals. *Chem. Phys. Lett.* **29**, 163–168 (1974).
51. C. C. Felix, R. C. Sealy, Photolysis of melanin precursors: Formation of semiquinone radicals and their complexation with diamagnetic ions. *Photochem. Photobiol.* **34**, 423–429 (1981).
52. L. Michaelis, G. F. Boeker, R. K. Reber, The paramagnetism of the semiquinone of phenanthrenequinone-3-sulfonate. *J. Am. Chem. Soc.* **60**, 202–204 (1938).
53. L. Pauling, *The Nature of the Chemical Bond* (Cornell Univ. Press, ed. 3, 1960).
54. P. S. Rao, E. Hayon, Ionization constants and spectral characteristics of some semiquinone radicals in aqueous solution. *J. Phys. Chem.* **77**, 2274–2276 (1973).

Acknowledgments: We note with sadness that our friend and colleague G.R.H. passed away while the manuscript was in draft. We acknowledge G. Schenk's help in the use of his laboratory and discussions with J. Harmer. The Supplementary Material is available free of charge. **Funding:** P.M. is a Sêr Cymru Research Chair and was formally an Australian Research Council (ARC) Discovery Outstanding Research Award Fellow. The work was funded through the ARC Discovery Program (DP140103653) and the Sêr Cymru Program (European Regional Development Fund and Welsh European Funding Office). A.B.M. was funded by the ARC Discovery Program. S.B.R. was funded by the University of Queensland International Scholarship. The Centre for Organic Photonics is a strategic initiative of the University of Queensland. **Author contributions:** A.B.M., S.B.R., and C.N. developed the photo-EPR/photoconductivity technique. S.B.R. and C.N. obtained the ambient photo-EPR/photoconductivity data. A.B.M. obtained the hydration-dependent photo-EPR and photoconductivity data with associated CW EPR spectra. High–microwave power CW EPR was obtained by S.B.R., C.N., and G.R.H. Uncertainty analysis was performed by A.B.M. Direction of project was performed by G.R.H., P.M., and A.B.M. Interpretation of the results was performed by all authors. Writing of the manuscript was performed by all authors. **Competing interests:** The authors declare that they have no competing interests. **Data and materials availability:** All data needed to evaluate the conclusions in the paper are present in the paper and/or the Supplementary Materials. Additional data related to this paper may be requested from the authors.

Submitted 4 October 2017
Accepted 13 February 2018
Published 28 March 2018
10.1126/sciadv.aaq1293

Citation: A. B. Mostert, S. B. Rienecker, C. Noble, G. R. Hanson, P. Meredith, The photoreactive free radical in eumelanin. *Sci. Adv.* **4**, eaaq1293 (2018).

Science Advances

The photoreactive free radical in eumelanin

Albertus B. Mostert, Shermiyah B. Rienecker, Christopher Noble, Graeme R. Hanson and Paul Meredith

Sci Adv **4** (3), eaaq1293.
DOI: 10.1126/sciadv.aaq1293

Science Advances (ISSN 2375-2548) is published by the American Association for the Advancement of Science, 1200 New York Avenue NW, Washington, DC 20005. The title *Science Advances* is a registered trademark of AAAS.